# Prognostic biomarker NRG2 correlates with autophagy and epithelial-mesenchymal transition in breast cancer

RUIJIE ZHOU[1*], JINJIN DAI[1*], RUNLONG ZHOU[1*], MENGYI WANG[1], XIAOTONG DENG[1], QING ZHUO[1], ZHENRONG WANG[1], FAN LI[2], DI YAO[1] and YAO XU[1]

[1]Institute of Biology and Medicine, College of Life Science and Health, Wuhan University of Science and Technology, Wuhan, Hubei 430081; [2]Wuhan Bio-Raid Biotechnology Co., Ltd., Wuhan, Hubei 430075, P.R. China

Received December 14, 2023; Accepted March 5, 2024

DOI: 10.3892/ol.2024.14410

**Abstract.** Breast cancer (BRCA) is a leading cause of death in women worldwide, accounting for 31% of female cancer. Autophagy plays a crucial role in cancer progression, however, the function of autophagy-related gene neuroregulatory protein 2 (NRG2) in BRCA and its underlying molecular mechanisms remain unclear. In the present study, the expression of the NRG2 gene in BRCA was significantly down-regulated compared with the normal controls. The low expression level of NRG2 was related to poor survival rate of BRCA. The receiver operating characteristic curve of NRG2 showed a good diagnostic value for distinguishing BRCA from normal tissues (AUC=0.932). GO-KEGG analysis and GSEA enrichment analysis showed that NRG2 and its regulated genes were enriched in autophagy-related and immune-related pathways, and NRG2 was positively correlated with a number of immune cells and immune checkpoint genes. In addition, knockdown of NRG2 significantly promoted the proliferation, invasion and migration of BRCA cells. The autophagy marker, LC3-II and epithelial-mesenchymal transition (EMT) marker, vimentin were increased, while P62 and E-cadherin were decreased in response to NRG2 depletion. The findings of the present study demonstrated that NRG2 acts as a tumor suppressor factor that contributes to the immune escape and anti-tumor immunity inhibition by regulating the pathological process of autophagy and EMT, suggesting that NRG2 could be used as a prognostic biomarker and clinical target for BRCA therapy.

*Correspondence to:* Professor Yao Xu, Institute of Biology and Medicine, College of Life Science and Health, Wuhan University of Science and Technology, 2 Huangjiahu West Road, Wuhan, Hubei 430081, P.R. China
E-mail: xuyao0307@wust.edu.cn

*Contributed equally

*Key words:* neuroregulatory protein 2, biomarker, autophagy, epithelial-mesenchymal transition, breast cancer

## Introduction

Breast cancer (BRCA) has become the most prevalent cancer in women, with ~20,000 new cases reported each year, making it the primary cause of cancer deaths in women worldwide (1-3). Based on the International Agency for Research on Cancer reports, BRCA has accounted for 31% of all malignancies in women by 2023 (4). The available clinical strategies for the treatment of BRCA include surgical excision, radiotherapy, endocrine therapy, immunotherapy and targeted therapy, however, due to residual tumors and drug resistance, patients with BRCA still generally have a poor prognosis and the rate of relapse remains high (5). Therefore, it is crucial to explore the molecular mechanisms of BRCA development to identify significantly effective therapeutic targets and prognostic indicators.

Autophagy is a conserved intracellular, degrative process that is activated in response to various stressors and regulated by evolutionarily conserved autophagy-related genes (ATGs) (6,7). Under conditions of nutrient starvation, cells undergo a lysosomal-dependent self-digestive process in which cytoplasmic components, including damaged proteins and organelles, are hydrolyzed to produce nutrients and energy necessary for cell maintenance (8). Previous studies reported that autophagy plays a dual role in cancer development whereby it can inhibit metastasis in the early stage of tumorigenesis, while promoting tumor progression by increasing cell growth, proliferation and survival in the late stage (6,9,10). Therefore, the function of autophagy may depend on the oncogenic driving factor.

Recent studies have revealed a reciprocal interplay between epithelial-mesenchymal transition (EMT) and autophagy-related signaling pathways (11-13). EMT-induced autophagy is considered a novel mechanism that regulates the cytotoxic activity of T-lymphocytes and tumors in BRCA, and the tumor cells undergoing EMT display tumor resistance associated with autophagy induction (14). A previous study reported that autophagy induced by heat treatment upregulated TGF-β signaling activity and promoted the EMT phenotype, thereby enhancing the metastasis ability in BRCA (15). Thus, the key factors that are associated with EMT and autophagic processes could be utilized as prognostic markers or drug targets for BRCA therapy.

The Human Autophagy Database (HADb; http://www.autophagy.lu/index.html) showed that neuroregulatory protein 2 (NRG2) is an autophagy-related gene, and plays an critical role in malignant tumorigenesis of various human cancer types, such as breast (16), prostate (17), and lung (18) cancer. NRGs activate the ErbB tyrosine kinase receptor family members, which can initiate a variety of downstream signal transduction pathways related to cell proliferation and differentiation, apoptosis, migration and adhesion (19). Zhao *et al* (20) reported that NRG2 was highly expressed in glioma tissues of different grades, which may partially regulate the expression of GFAP in glioma cells through Akt signaling, thus affecting the survival rate of patients. Previous studies investigated that NRG2 participated in the development of ATGs involved in the prognostic signature for gastric cancer and prostate cancer (21,22). However, there is a lack of research focusing on the role of NRG2 in BRCA.

In the present study, an autophagy-related prognostic model was constructed utilizing The Cancer Genome Atlas (TCGA) database (https://portal.gdc.cancer.gov/) and a hub gene was selected for further study. The biological function and immune cell infiltration of the NRG2 gene were analyzed by bioinformatics and the ability of NRG2 to regulate autophagy and EMT was determined by *in vitro* experiments.

## Materials and methods

*Data*. Through the HADb, 222 ATGs were found. The dataset from TCGA-BRCA (phs000178) was used for the analysis. The 'DESeq2' package in R (version 4.1.1, https://www.r-project.org/) (23) was employed to conduct differentially expressed gene (DEG) analysis in both groups. A total of 10,935 DEGs with significant statistical differences were selected when the threshold value was set at |log2FC|>1 and P<0.01.

*Definition of the autophagy-related prognostic model*. Univariate Cox regression analysis was performed using survival (version 3.2.10; https://CRAN.R-project.org/package=survival) and rms (version 6.3-0; https://hbiostat.org/R/rms/), and the futime and fustat of two cohorts of patients in all BRCA samples were compared. From 31 intersecting genes, 10 prognostic ATGs were identified (P<0.2).

*Construction of autophagy-related prognostic model in BRCA*. Lasso regression was used to create a prognostic signature utilizing the samples from the TCGA cohort. Multiple Cox regression analysis was performed using survival (version 3.2.10) and rms (version 6.3-0) to identify if the marker genes may function as stand-alone predictors of patient survival. The regression coefficients (β) from the multivariate Cox regression model were combined with the relevant gene expression levels to generate a multi-gene marker-based predictive risk score. TCGA data was used to train the risk score model, which was built using glmnet (version 4.1.7) as follows: Risk score=expression level of interferon-γ (IFNG) x (-0.17421391598924) + expression level of neuregulin 1 (NRG1) x (-0.110265298892829) + expression level of NRG2 x (0.0562837346428505) + expression level of c-FOS x (-0.014540998384746) + expression level of eukaryotic translation initiation factor 4E-binding protein 1 (EIF4EBP1) x (0.124693974397309). The median risk score was regarded as the cut-off value to partition the cohort of patients with BRCA from TCGA into high-risk and low-risk groups. Kaplan-Meier (KM) survival curves were conducted with a two-sided log-rank test, and P<0.05 was considered to indicate a significant difference. Time-dependent receiver operating characteristic (ROC) curve analyses were conducted to evaluate the predictive capability of the model; the closer the AUC was to 1, the better the diagnosis. AUC values of 0.5-0.7 represented a low accuracy, 0.7-0.9 represented a moderate accuracy and >0.9 represented a high accuracy.

*Identification of hub gene*. Protein-protein interaction (PPI) analysis of 31 differentially expressed autophagy-related genes (DEATGs) was performed using STRING database (https://cn.string-db.org/). The Cytoscape (version 3.9.1) (24) plugin CytoHubba (25) was used to identify hub genes in the module subnet, while Clustering Coefficient methods were utilized to identify hub genes.

*Gene expression and clinicopathological character analysis*. BRCA in TCGA [paraneoplastic (n=113); tumor (n=1,113)], GSE26304 [normal (n=6); cancer (n=109)] (26) and GSE45827 [normal (n=11); cancer (n=144)] (27) from the Gene Expression Omnibus (GEO, https://www.ncbi.nlm.nih.gov/geo/) public database were selected for differential analysis. Clinical and gene expression data [including T-classification, M-classification, N-classification, age, ethnicity, estrogen receptor (ER), progesterone receptor (PR) and human epidermal growth factor receptor 2 (HER2) status of patients] were extracted from the TCGA database to explore NRG2 expression in different clinical subgroups of BRCA.

*Survival analysis*. Kaplan-Meier survival analysis was performed using the survival (version 3.2.10) and survminer (version 0.4.9; https://CRAN.R-project.org/package=survminer). TCGA-BRCA data (removing normal samples and samples without clinical information) was categorized into two groups based on high and low NRG2 expression levels. The prognostic impact of NRG2 was also assessed based on overall survival (OS), progression-free interval (PFI) and disease-specific survival (DSS). The diagnostic value of NRG2 was assessed using the pROC (version 1.18.0; https://rdocumentation.org/packages/pROC/versions/1.18.5) to generate ROC curves. Cox regression analysis was performed using the survival package and forest plot was visualized using ggplot2 (version 3.3.3; https://ggplot2.tidyverse.org).

*Functional clustering analysis*. Spearman correlation analysis of NRG2 was performed using the LinkedOmics database (http://www.linkedomics.org/login.php) (28), a total of 13,455 genes were screened according to P<0.01. Genes with absolute values of correlation coefficients >0.3 were subjected to Gene Ontology (GO) and Kyoto Encyclopedia of Genes and Genomes (KEGG) enrichment analysis using the clusterProfiler (version 4.4.4) (29) and visualized using the ggplot2 package. The BRCA data in TCGA were divided into high and low expression groups based on NRG2 level, and the low expression group was used as the control for difference analysis, and the genes with P<0.01 were selected as the

analysis list for Gene Set Enrichment Analysis (GSEA) enrichment analysis. GSEA was performed using c2.cp.reactome.v2022.1.Hs.symbols.gmt (Reactome Pathway Database) and h.all.v7.5.1.symbols.gmt (Hallmarks). Genes with P<0.01 and |log2FC|>2 were selected as the analysis list for GO-KEGG enrichment analysis associated with log2FC which was performed with the clusterProfiler. Log2FC was used to calculate the Zscore value corresponding to each enriched pathway via the GOplot (version1.0.2) (30).

*Immunity analysis*. Correlation between NRG2 and immune infiltration matrix data of 24 immune cells (31) was assessed by the ssGSEA (Single Sample Gene Set Enrichment Analysis) of the R package GSVA (version 1.46.0) (32). Spearman correlation analysis was used to identify the relationship between NRG2 expression and the expression of immune checkpoint genes (PDCD1, CD274, HAVCR2, TIGIT, SIGLEC15, CTLA4, LAG3 and PDCD1LG2). The chemokine and receptor related with NRG2 was analyzed by the tumor and immune system interaction database (TISIDB; http://cis.hku.hk/TISIDB/) (33).

*Cell culture*. MDA-MB-231 and 293T cells were obtained from the American Type Culture Collection. Cells were cultured in Dulbecco's Modified Eagle Medium (DMEM; Gibco; Thermo Fisher Scientific, Inc.) supplemented with 10% FBS (Every Green; Zhejiang Tianhang Biotechnology Co., Ltd.) and 1% penicillin/streptomycin (Dalian Meilun Biology Technology Co., Ltd.), and incubated at 37˚C and 5% $CO_2$ in a humidified equipment.

*Stable cell line screening*. The short hairpin RNA-mediated RNA interference assay was established to induce knockdown of NRG2 in MDA-MB-231 cells. First, three small interfering (si) RNA oligonucleotides targeting the NRG2 coding sequence were designed with the following sequences: siRNA-1: 5'-GCCGAGACATTCGCATCAAAT-3', siRNA-2: 5'-GCAGCGGCTCGGGCGGCGGCT-3', siRNA-3: 5'-TCG GCGTCGGACGACGACG CG-3', and the scrambled negative control: 5'-TCGTGATCAATCACAGGCACA-3'. The siRNA sequences were synthesized by Beijing Tsingke Biotech Co., Ltd. Each of the siRNAs (50 nM) was transiently transfected into MDA-MB-231 cells in 6-well plate using Lipofectamine 2000® (Thermo Fisher Scientific, Inc.; cat. no. 11668019) at 37˚C for 24 h to determine its knockdown efficiency. Then, the lentivirus vector plko.1 (Promega Corporation) with siRNA sequences was constructed (plko.1-shNRG2 or plko.1-sh-control), and prepared for lentivirus packaging. The plasmid (plko.1-shNRG2 or plko.1-sh-control), pCMV-VSV-G (Promega Corporation) and pCMV-Gag-Pol (Promega Corporation) was used at a 4:3:1 ratio (12 $\mu$g total DNA in a 10-cm dish) were cotransfected into 293T cells using PEI reagent (Polyplus-transfection SA). After 72 h of incubation at 37˚C, viral supernatant was collected and filtered through a 0.22-$\mu$m filter. The virus titer was determined using a Lenti-Pac™ HIV qRT-PCR Titration Kit (GeneCopoeia, Inc.), and then the virus was used to infect MDA-MB-231 cells at the multiplicity of infection of 5. Puromycin (1 $\mu$g/ml) was used to screen stable MDA-MB-231 cells with NRG2 silence or the control group after lentiviral infection. The efficiency of NRG2 silencing was evaluated using inverted fluorescence microscopy ($GFP^+$) and reverse transcription-quantitative PCR (RT-qPCR) 5 days after infection.

*RT-qPCR*. Total RNA was extracted using Ultrapure RNA Kit (CWBio) from cells. Reverse Hifair® III 1st Strand cDNA Synthesis SuperMix (Shanghai Yeasen Biotechnology Co., Ltd.) was used to reverse transcribe the total RNA into complementary DNA (cDNA) according to manufacturer's protocol. After which, the qPCR assay was performed using 2x Universal SYBR Green (ABclonal Biotech Co., Ltd.). The instrument for qPCR was CFX Connect Real-Time PCR Detection System (Bio-Rad) with the following conditions: 40 cycles of 95˚C for 10 sec, 60˚C for 20 sec and 72˚C for 15 sec were performed after 10 min at 95˚C. The $2^{-\Delta\Delta Cq}$ method was used to calculate the relative expression (34). GAPDH was regarded as the internal control to standardize the results. Primer sequences were as follows: NRG2-forward (F): 5'-ACA GCGGAAGCAGATGCAC-3', reverse (R): 5'-GTTTCTCTC CTGATGACATGGTC-3'; GAPDH-F: 5'-TGCACCACCAAC TGCT TAGC-3', R: 5'-GGCATGGACTGTGGTCATGAG-3'.

*Cell proliferation assays*. Cell counting kit-8 (CCK-8) assay was used to assess cell proliferation. Cells were attached to 96-well plate at indicated times and cell viability was measured by adding CCK8 reagents (Dalian Meilun Biology Technology Co., Ltd.) with incubation for 2 h. The OD450 value of each sample was quantified using a spectrophotometer. Cell proliferation was also evaluated by a colony formation assay. MDA-MB-231 cells were plated at a low density ($2x10^3$ cells/well) in 6-well plate, and culture media with 30% serum (Every Green; Zhejiang Tianhang Biotechnology Co., Ltd. was replaced every 3 days. Following 2 weeks of incubation, 4% paraformaldehyde (Dalian Meilun Biology Technology Co., Ltd.), was used to fix the cells at room temperature for 30 min. After staining with 0.1% crystal violet (Servicebio) for 15 min at room temperature, excess crystal violet was washed away with PBS, and the plaques were imaged and analyzed using the ImageJ software (version 1.54f; National Institutes of Health).

*Transwell assay*. First, 50 $\mu$l of DMEM-diluted Ceturegel® Matrix LDEV-Free (Shanghai Yeasen Biotechnology Co., Ltd.) was added to each well of the Transwell inserts (Labselect; Beijing Lanjieke Technology Co., Ltd.) and incubated at 37˚C for 1 h. A volume of 500 $\mu$l of complete medium (DMEM supplemented with 10% FBS) was plated to the bottom chamber as a chemoattractant, and $1x10^5$ cells/well were seeded in the upper chamber in 100 $\mu$l of serum-free medium. After incubation at 37˚C for 12 h, the cells remaining at the upper membrane were removed by washing with PBS, and the cells on the lower membrane were fixed with 4% paraformaldehyde at room temperature for 30 min and stained with 1X Modified Giemsa stain (Beyotime Institute of Biotechnology) at room temperature for 45 min, and then images were captured using the inverted fluorescence microscope.

*Cell wound healing assay*. A total of $1x10^5$ cells/well were grown with complete medium in a 6-well plate. Upon reaching 75% confluence, the cell layers were scratched using a sterile pipette tip, and washed with PBS to remove cell debris. After

which, the cells were cultured at 37˚C for 72 h in serum-free medium, and the healing process was recorded using an inverted fluorescent microscope. The wound healing was assessed using the closure rate, which was calculated as follows: [(Wound area at 0 h-wound area at indicated h)/wound area at 0 h] x100%.

*Western blotting*. Total cell proteins were extracted from the harvested cells using RIPA lysis buffer (Beyotime Institute of Biotechnology) and PMSF (Beyotime Institute of Biotechnology). The protein concentration in the supernatants was quantified by BCA detection assay (cat. no. P0010S; Beyotime Institute of Biotechnology). The Omni-Easy™ One-step Color PAGE Gel Rapid Preparation Kit (Epizym, Inc.; cat. nos. PG211 and PG213) was used to prepare 7.5 and 12.5% gels. Aliquots containing 20 $\mu$g total protein were fractionated by SDS-PAGE gel electrophoresis and blotted onto a PVDF membrane (cat. no. IPVH00010; MilliporeSigma). The membrane was blocked for 1 h at room temperature with 5% non-fat milk, and was incubated with primary antibodies at 4˚C overnight. The membrane was washed and incubated for 1 h at room temperature with secondary antibodies, and the expression of proteins was visualized using the ECL developing solution (Biosharp Life Sciences; cat. no. BL520A). Primary antibodies used in the present study were as follows: mouse anti-GAPDH (1:5,000; ABclonal Biotech Co., Ltd.; cat. no. AC033), rabbit anti-LC3B (1:1,000; ABclonal Biotech Co., Ltd.; cat. no. A11282), rabbit anti-P62 (1:2,000; ABclonal Biotech Co., Ltd.; cat. no. A19700), rat anti-E-cadherin (1:500; Santa Cruz Biotechnology, Inc.; cat. no. sc-59778) and mouse anti-Vimentin (1:500; Santa Cruz Biotechnology, Inc.; cat. no. sc-373717); and the secondary antibodies were as follows: HRP Goat Anti-Rat IgG (H+L; 1:10,000; ABclonal Biotech Co., Ltd.; cat. no. AS028), HRP Goat Anti-Mouse IgG (H+L; 1:10,000; ABclonal Biotech Co., Ltd.; cat. no. AS003) and HRP Goat Anti-Rabbit IgG (H+L; 1:10,000; ABclonal Biotech Co., Ltd.; cat. no. AS014). The gray value was measured and quantified by ImageJ software (version 1.54f; National Institutes of Health).

*Immunofluorescence*. Cells were grown on cell climbing slices until reaching ~80% confluence, after which 4% paraformaldehyde was used to fix the cells at room temperature for 30 min. The fixed cells were permeabilized with 0.1% Triton X-100 in PBS for 15 min at room temperature. Non-specific binding was reduced by incubating the cells with 5% BSA at room temperature for 1 h, and cells were with rabbit anti-LC3B (ABclonal Biotech Co., Ltd.; cat. no. A11282) and p62 (ABclonal Biotech Co., Ltd.; cat. no. A19700) antibodies (1:200) overnight at 4˚C. The next day, cells were incubated with secondary anti-rabbit-Cy3 conjugated antibody (1:200; Wuhan Servicebio Technology Co., Ltd.; cat. no. GB21303) at room temperature for 1 h. Nuclei were stained using 4',6-diamidino-2-phenylindole (DAPI; Beyotime Institute of Biotechnology) at room temperature for 10 min. Finally, slides were cover-slipped by water-soluble glycerol-based mounting medium and viewed on an inverted fluorescent microscope. The results of immunofluorescence assay were analyzed by ImageJ software (version 1.54f; National Institutes of Health).

*Statistical analysis*. All data analysis was performed using GraphPad Prism software (version 8.0.1; Dotmatics). The statistical differences in experimental groups were analyzed using unpaired student's t-test or one-way ANOVA with Tukey's post hoc test. Each treatment of cell samples was replicated at least three times. Data are presented as mean ± standard error of the mean. $P<0.05$ was considered to indicate a statistically significant difference.

## Results

*Construction of autophagy-related prognostic model for breast invasive carcinoma*. Different expressions of ATGs were analyzed using $P<0.01$ and $FC>1$ thresholds (Fig. 1A and B). According to the cox regression analysis results, among 31 DEATGs, 10 genes associated with the prognosis of patients were identified ($P<0.2$; Fig. 1C). The LASSO logistic regression indicated an autophagy risk score model composed of seven genes: TP63, PTK6, IFNG, NRG1, NRG2, FOS and EIF4EBP1 (Fig. 1D and E). In addition, the model was examined using ROC curves to assess the diagnostic utility of the autophagy model in the TCGA-BRCA cohort (Fig. 1F). The distributions of the risk scores, survival time, survival status and expression patterns of 7 genes are displayed in Fig. 1G. Subsequently, a PPI network of 31 DEATGs was constructed (Fig. 1H), and the hub genes were screened by the Cytohubba plugin of Cytoscape (Table SI). The results showed that NRG2 was the gene with higher clustering coefficient scores in the autophagy risk model than the scores of PTK6 and NRG1, suggesting that it may play a significant role in the nosogenesis of BRCA associated with autophagy.

*Expression of NRG2 in pan-cancer and BRCA*. In light of the significance of NRG2 in the autophagy-related prognosis model of BRCA, a comprehensive investigation of NRG2 was conducted. The pan-cancer expression analysis showed that NRG2 expression was significantly lower than normal tissue in cancers such as BLCA, BRCA, CESC and COAD ($P<0.01$; Fig. 2A). The transcriptional mRNA level of NRG2 in BRCA was analyzed based on TCGA and GEO data, with a significant down-regulation in BRCA tissues compared with normal tissues found ($P<0.001$; Fig. 2B). Clinical (including T-classification, M-classification, N-classification, age, ethnicity, PR, ER and HER2 status of patients) and gene expression data were extracted from TCGA to explore the expression of NRG2 in different clinical subgroups of BRCA (Table SII). The results indicated significant differences in the expression of NRG2 among age and ethnicity, while no significant variance was observed across stages of TMN classification (Fig. 2C-G). In addition, it was found that the expression of NRG2 was negatively associated with the status of PR, ER and HER2 (Fig. 2H-J). Based on the results, further analyses were conducted to determine the expression level of NRG2 among distinct subtypes of BRCA, and the significant prognostic ($P<0.05$) and diagnostic (AUC=0.972) value of NRG2 was found, specifically in Luminal B subtype of BRCA comparing with other BRCA types (Fig. S1).

*Association between NRG2 expression and prognosis of patients with BRCA*. To determine whether the NRG2 level

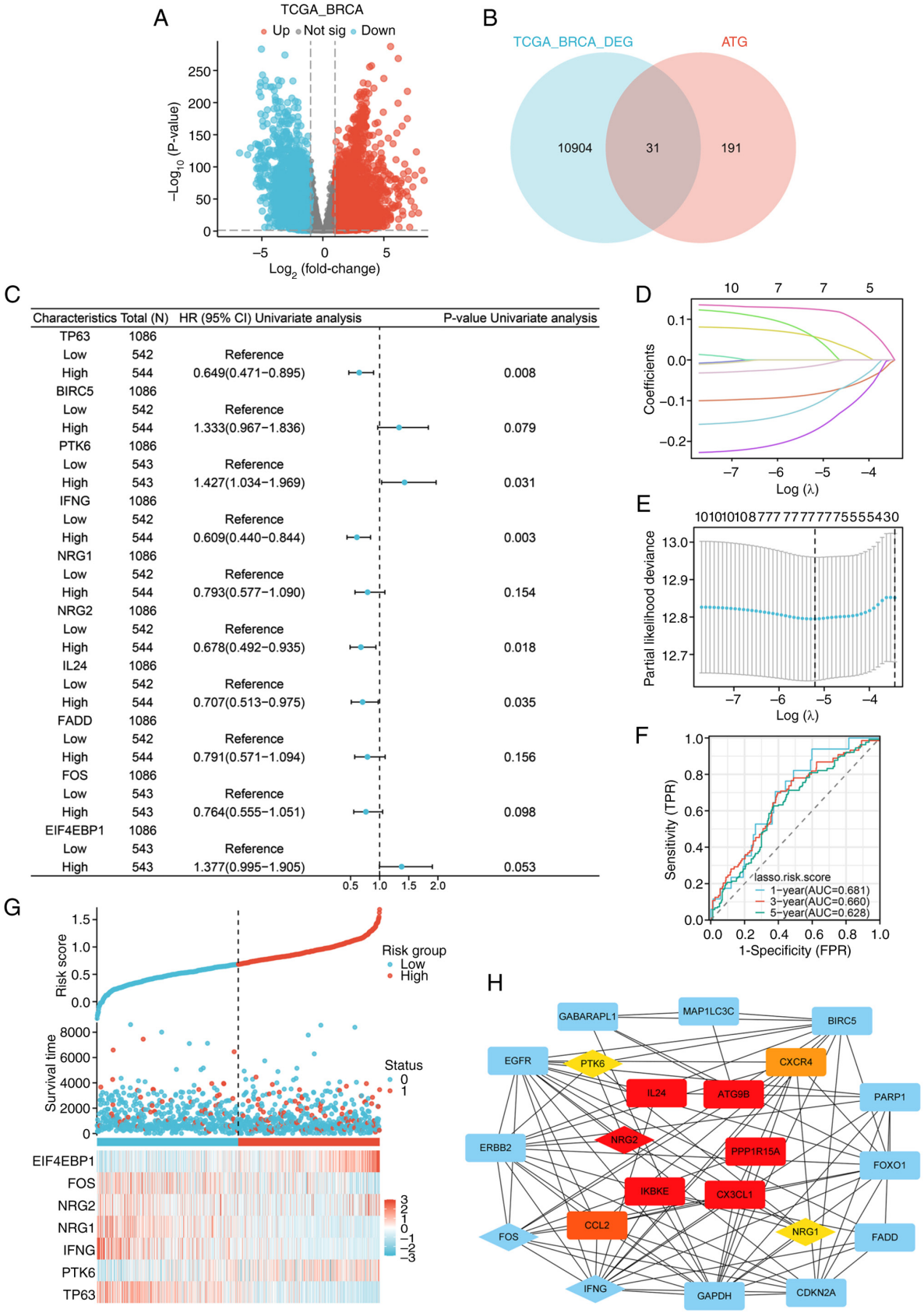


Figure 1. Construction of a prognostic autophagy model for BRCA. (A) Volcano map of the DEGs in TCGA-BRCA (P<0.01, |log2FC|>1). (B) Venn diagram of DEGs and ATGs. (C) Forest map of univariate cox regression analysis (P<0.2). (D) Lasso coefficient spectrum of seven autophagy-related genes. (E) Cross-validation of adjustment parameter selection in a proportional hazards model. (F) ROC curves of the autophagy risk model from the TCGA-BRCA cohort. (G) Distribution of the risk score, survival status and expression profiles of seven genes in TCGA set. (H) PPI network of 31 DEATGs, with the genes in the autophagy-related prognostic model displayed by diamonds, and the top ten genes with the highest clustering coefficient scores were displayed in red (high), orange (moderate) and yellow (low) based on their scores, respectively. BRCA, breast cancer; DEGs, differential expressed genes ATGs, autophagy-related genes; ROC, receiver operating characteristic; TCGA, The Cancer Genome Atlas; PPI, protein-protein interaction; DEATGs, different expression of autophagy-related genes.

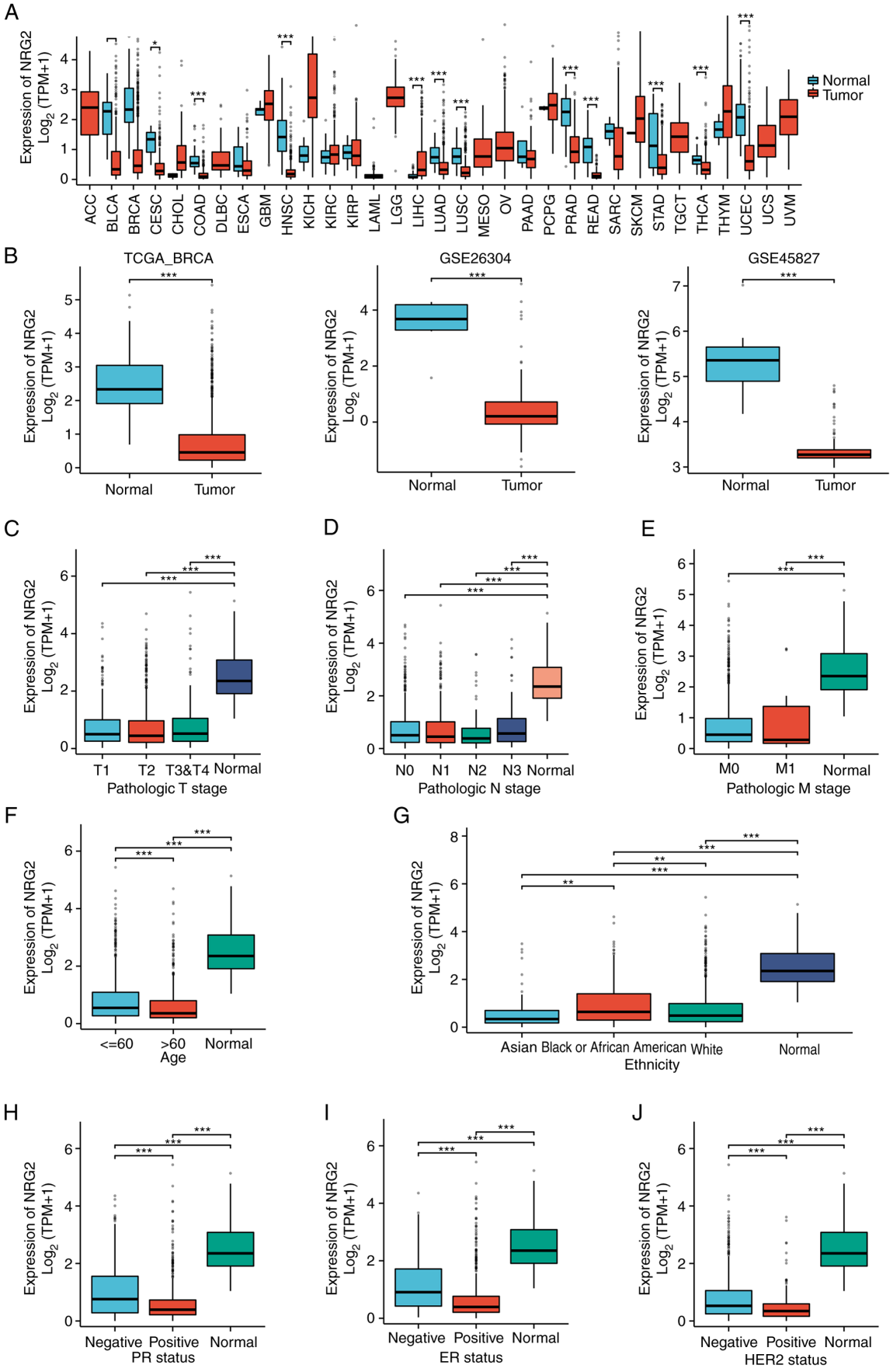


Figure 2. NRG2 expression in pan-cancer and BRCA. (A) NRG2 expression in pan-cancer based on TCGA database. (B) NRG2 expression in BRCA based on TCGA database and the GEO database. (C-J) Relationship between NRG2 expression levels and clinicopathological characteristics of patients with BRCA: (C) T-stage; (D) N-stage; (E) M-stage; (F) age; (G) ethnicity; (H) PR status; (I) ER status; and (J) HER2 status. NRG2, neuroregulatory protein 2; BRCA, breast cancer; TCGA, The Cancer Genome Atlas; GEO, Gene Expression Omnibus; PR, progesterone receptor; ER, estrogen receptor; HER2, human epidermal growth factor receptor 2; ns, no significance. $^{*}$P<0.05, $^{**}$P<0.01 and $^{***}$P<0.001.

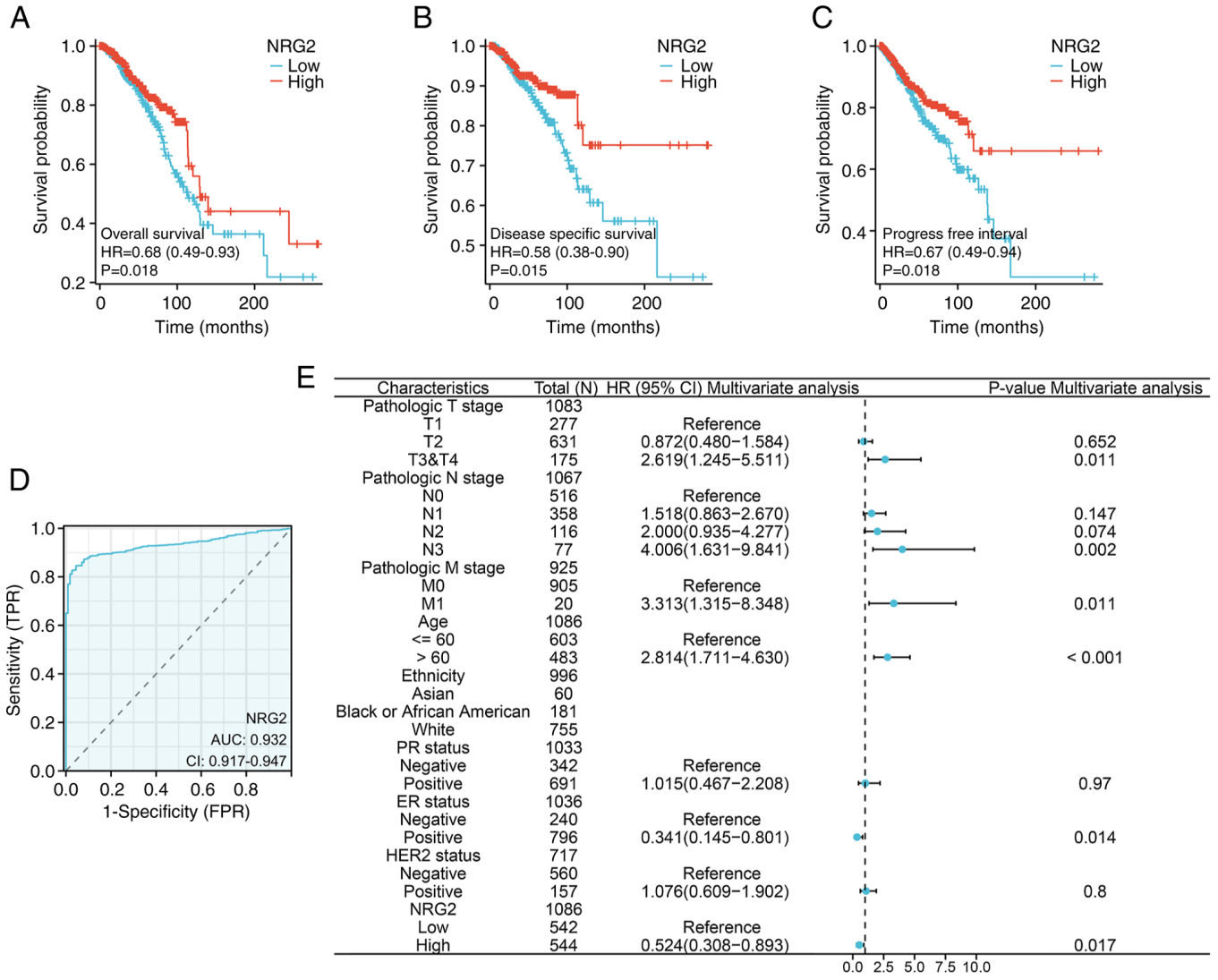


Figure 3. Effect of NRG2 expression on the prognosis of patients with BRCA and its diagnostic value. (A) Kaplan-Meier analysis for OS, (B) DSS and (C) PFI. (D) ROC curve. (E) Forest plot of multivariate cox regression analysis between clinical parameters, NRG2 expression and OS of patients. NRG2, neuroregulatory protein 2; BRCA, breast cancer; OS, overall survival; DSS, disease-specific survival; PFI, progression-free interval; ROC, receiver operating characteristic.

impacted the clinical outcomes of patients with BRCA, a prognostic model was constructed using KM survival curves. The results revealed that patients with low NRG2 expression had significantly poor OS, PFI and DSS compared with patients with high NRG2 levels (Fig. 3A-C; P<0.05). Additionally, the diagnostic value of NRG2 expression was evaluated using a ROC curve, and the AUC was calculated as 0.932, indicating that NRG2 had high accuracy in predicting outcomes (Fig. 3D). In univariate and multivariate Cox regression analyses, risk scores were found to be associated with OS. The multivariable Cox analysis revealed that advanced tumor stages (T3 & T4), lymph node involvement (N3), distant metastasis (M1), older age, ER-negative status and low expression of NRG2 were independent risk factors influencing OS in BRCA (P<0.05; Fig. 3E).

*Gene set enrichment analysis of NRG2 related and co-expressed genes*. To clarify the function of NRG2, related analysis of NRG2 was performed using the LinkedOmics database, and a total of 13,455 genes were detected (P<0.01; Figs. S2-S4), in which 833 biological processes (BP), 43 cellular components (CC), 108 molecular functions (MF) and 48 KEGG signaling pathways were obtained in GO-KEGG enrichment analysis. The enrichment analysis showed that NRG2 related genes were significantly enriched in BP such as mononuclear cell differentiation, lymphocyte differentiation and leukocyte cell-cell adhesion (Fig. 4A); for CC analysis, NRG2 and its related genes were located in regions such as the external side of the plasma membrane and cell-cell junctions (Fig. 4B); for MF analysis, NRG2 related genes were significantly enriched in several functions including signaling receptor activator activity and passive transmembrane transport activity (Fig. 4C); KEGG enrichment analysis showed that NRG2 and its related genes were mainly enriched in the Ras, JAK-STAT, Wnt, TNF and NF-κB signaling pathways (Fig. 4D).

Gene set GO-KEGG enrichment analysis showed that keratinization, epidermis development and neuroactive

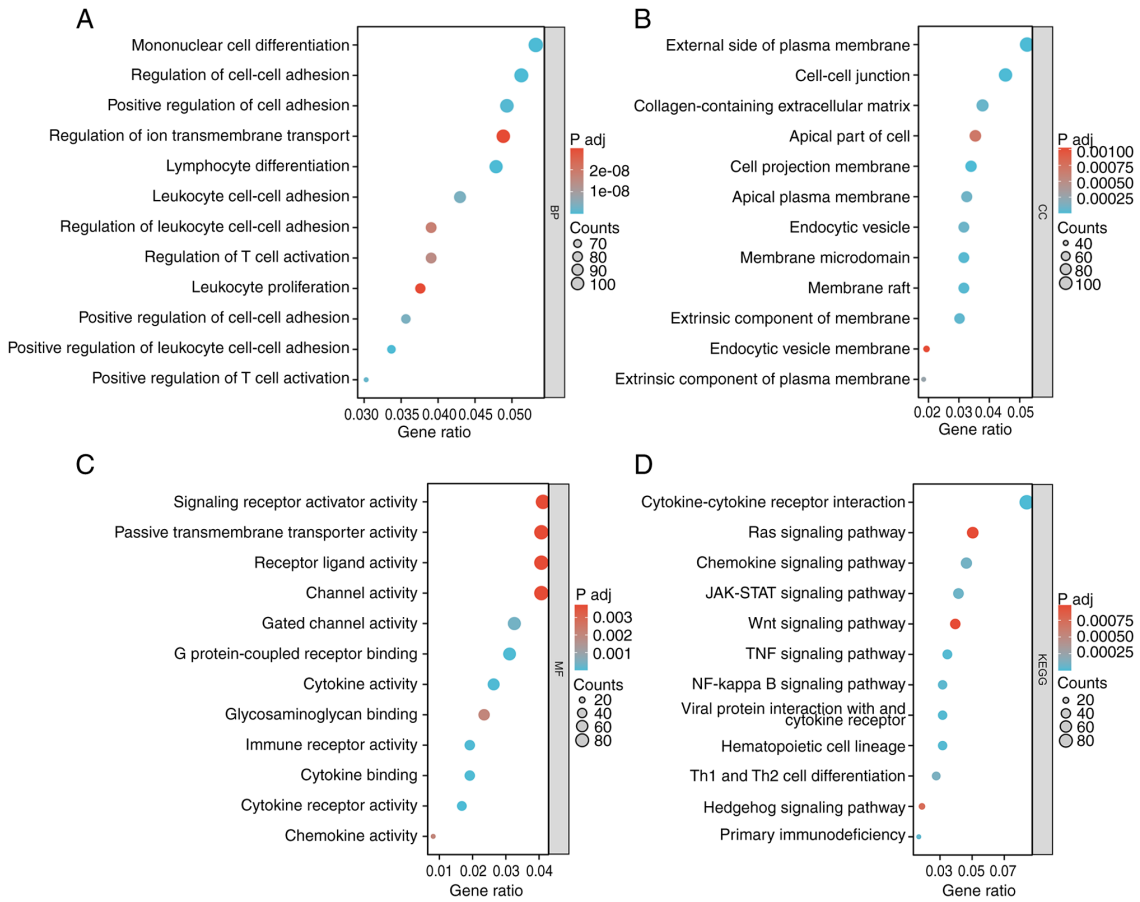


Figure 4. GO-KEGG enrichment analysis of NRG2 related genes. (A) BP of GO enrichment analysis of related genes of NRG2. (B) CC of GO enrichment analysis of related genes of NRG2. (C) MF of GO enrichment analysis of related genes of NRG2. (D) KEGG enrichment analysis of related genes of NRG2. GO, Gene Ontology; KEGG, Kyoto Encyclopedia of Genes and Genomes; NRG2, neuroregulatory protein 2; BP, biological process; CC, cellular component; MF, molecular function.

ligand-receptor interaction were significantly enriched in the NRG2 high-expression group (Fig. 5A). The enriched signaling pathways in the NRG2 high/low expression group were identified using the GSEA assay. GSEA analysis revealed a significant enrichment of keratinization, TNFα signaling via NF-κB, FCERI mediated MAPK activation and FCERI mediated NF-κB activation in the NRG2 high expression group, while oxidative phosphorylation was enriched in the NRG2 low expression group (Fig. 5B-F). Several representative pathways with high GSEA scores were selected and it was found that co-expression genes of NRG2 were involved in relevant processes such as immune response, nuclear DNA repair and transcription-related pathways (Fig. 5G-I).

*Relationship between NRG2 expression and immune indices.* Given the association between NRG2 and immunity, correlation analyses between the expression levels of NRG2 and immune infiltration matrix data in BRCA were performed. The majority of immune cell infiltration was positively related with NRG2 expression, while Th2 and Th17 cells were negatively related with NRG2 levels (Fig. 6A and C). Considering that NRG2 may act as a potential tumor suppressor gene in BRCA, the relationship between NRG2 and immune checkpoints (PDCD1, CD274, HAVCR2, TIGIT, SIGLEC15, CTLA4, LAG3 and PDCD1LG2) were further evaluated. NRG2 was found to be positively correlated with the expression levels of the majority of immune checkpoints (P<0.001; Fig. 6B). Moreover, it was further validated that NRG2 may positively regulate the chemokine-like CX3CL1 and CXCL family, specifically CXCL1-6, and may be positively associated with molecules including CCR2, CCR7 and CCR10 (Fig. 6D-E). These findings suggested that anti-tumoral immunity and immune escape may be involved in NRG2-mediated BRCA carcinogenesis.

*NRG2 knockdown facilitates cell proliferation, invasion and migration of MDA-MB-231 cells.* Based on bioinformatics analysis of the NRG2 gene, *in vitro* experiments were conducted to investigate its tumor inhibition effect in BRCA cells. The results of siRNA transient transfection revealed that siRNA-1 showed the best knockdown efficiency compared with the other two sequences, and was thus selected for subsequent stable cell screening (data not shown). The stable MDA-MB-231 cells with sh-NRG2 or sh-control were validated by RT-qPCR assay (Fig. 7A). CCK8 and colony formation assay showed that silencing of NRG2 significantly enhanced the proliferation ability of MDA-MB-231 cells (Fig. 7B-D). Transwell assay demonstrated a significant promotion in invasion capacity when the expression of NRG2 was decreased compared with the control group (Fig. 7E and F). Migration capability was

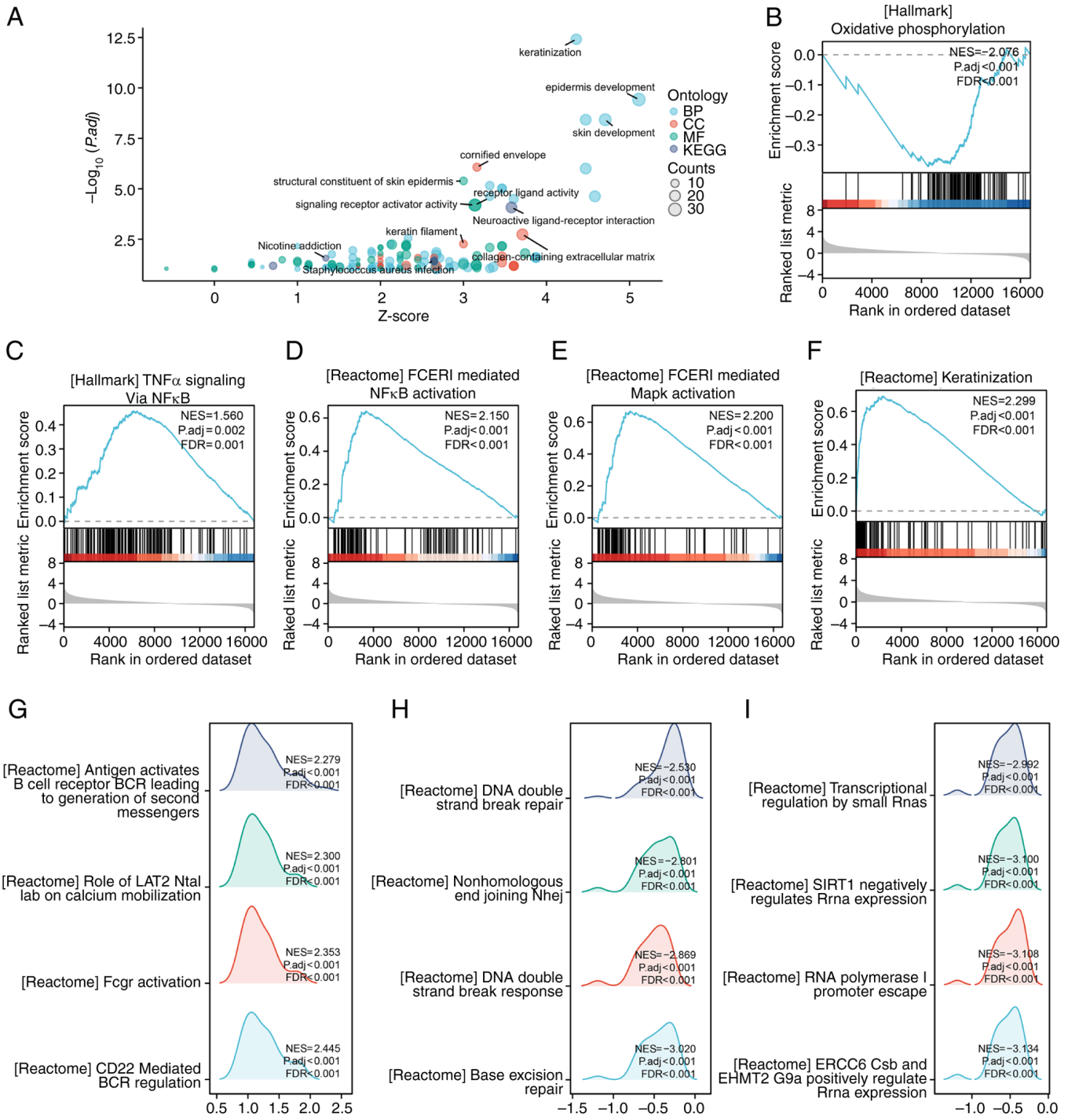


Figure 5. Gene set enrichment of NRG2 co-expression genes. (A) GO-KEGG enrichment analysis associated with log2FC. (B-F) Enrichment plots by GSEA: (B) Oxidative phosphorylation; (C) TNFα signaling via NFκB; (D) FCERI mediated MAPK activation; (E) FCERI mediated NFκB activation; and (F) keratinization. (G) Immunity-related GSEA pathways. (H) GSEA pathways associated with DNA damage repair. (I) Transcription-related GSEA pathways. NRG2, neuroregulatory protein 2; GO, Gene Ontology; KEGG, Kyoto Encyclopedia of Genes and Genomes; GSEA, gene set enrichment analysis; TNFα, tumor necrosis factor α; NFκB, nuclear factor κB; FCERI, high-affinity immunoglobulin E receptor; MAPK, mitogen-activated protein kinase.

quantified by calculating the area of cells migrating into the scratched part at 0, 24, 48 and 72 h (Fig. 7G-H), and the results revealed that the migration ability was significantly enhanced in the NRG2 knockdown group compared with the sh-control cells.

*NRG2 knockdown promotes autophagy and EMT.* Autophagic activity was evaluated by measuring autophagic protein expression (LC3 and P62) using western blotting and immunofluorescence. Elevated LC3-II and consumed P62 indicated an increased initiation of autophagy in response to NRG2 knockdown (Fig. 8A, B, E and F). Mesenchymal and epithelial state markers of EMT, vimentin and E-cadherin expression levels were detected to assess the EMT process. The results showed that upregulated vimentin and downregulated E-cadherin were identified in MDA-MB-231cells with

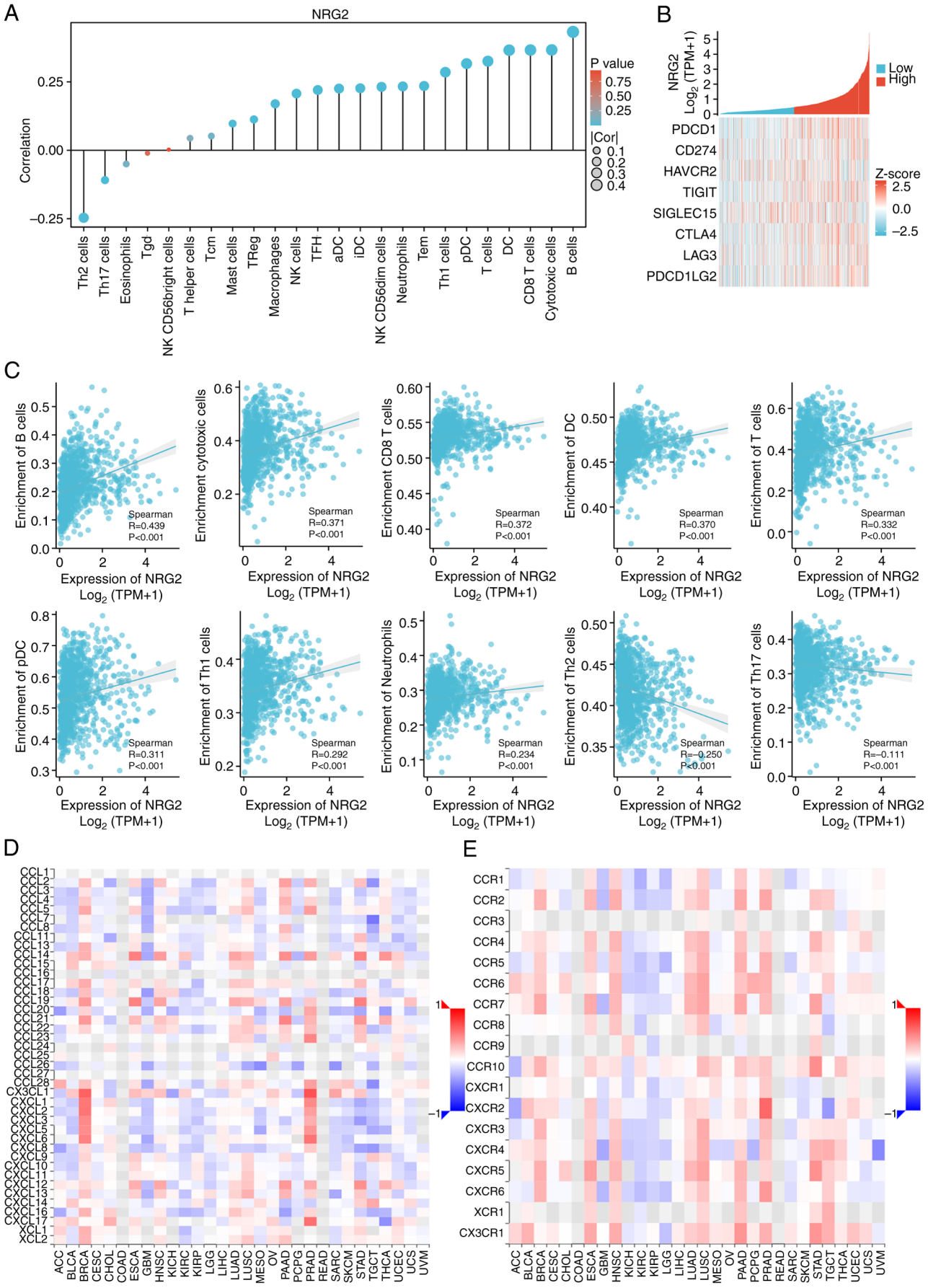


Figure 6. Correlation analysis of NRG2 with immune infiltrating cells and immune checkpoints. (A) Lollipop plot of immune infiltrates of NRG2 in BRCA. (B) Correlation heatmap between NRG2 and immune checkpoint related genes. (C) Scatter plots of correlation between NRG2 and immune cells. (D) Chemokines related to NRG2 in pan-cancer. (E) Chemokine receptor related to NRG2 in pan-cancer. NRG2, neuroregulatory protein 2; BRCA, breast cancer.

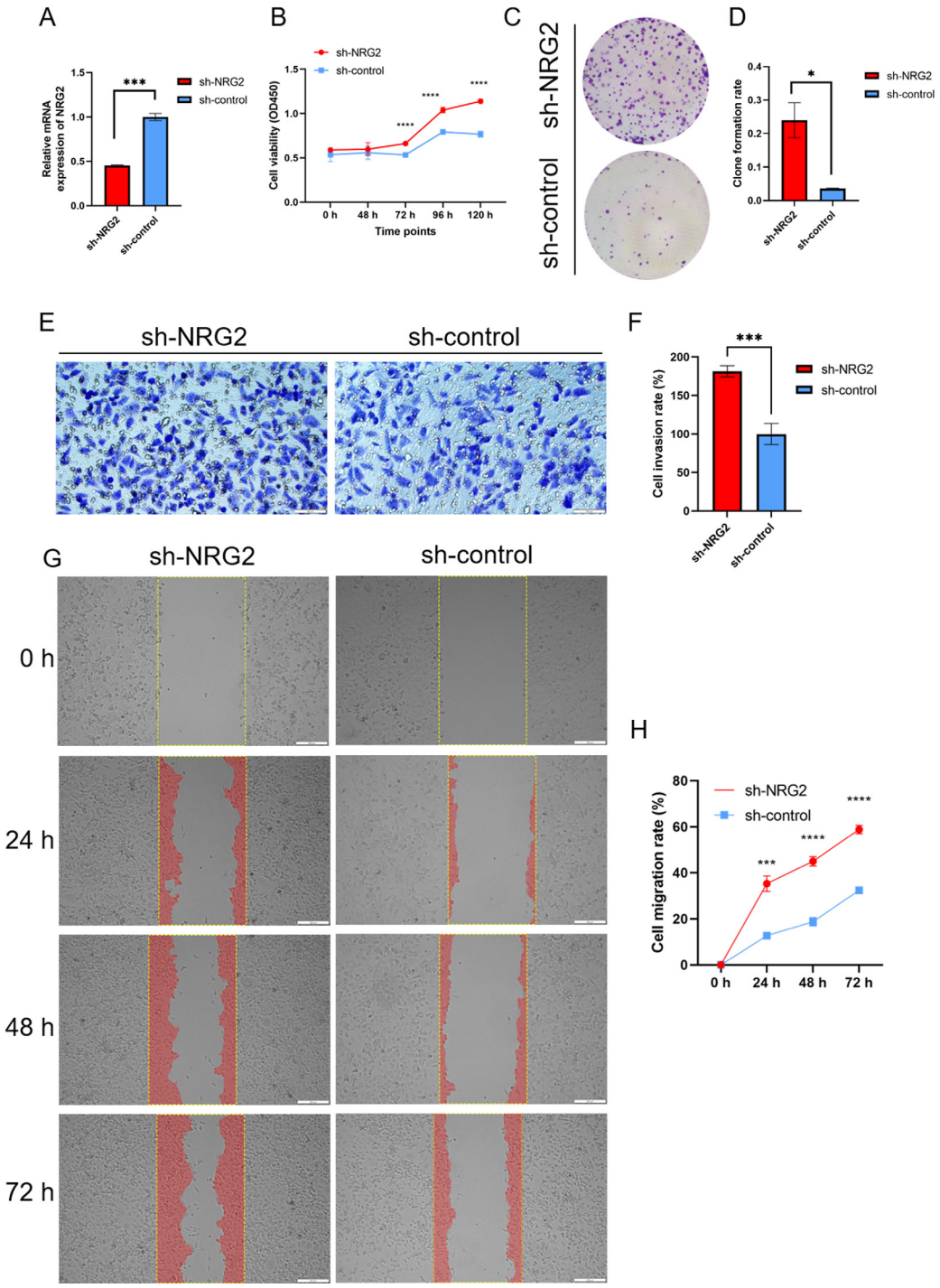


Figure 7. NRG2 is related to breast cancer cell proliferation, migration and invasion. (A) Estimation of the expression level of NRG2 in sh-NRG2 infected MDA-MB-231 cells and controls using RT-qPCR. (B) Cell proliferation in sh-NRG2 infected MDA-MB-231 cells and control was analyzed by CCK-8 assay. (C) Cell proliferation of sh-NRG2 infected MDA-MB-231 cells and control using the plate clone formation assay. (D) Quantitative results of C. (E) Knockdown of NRG2 increased MDA-MB-231 cell invasion as measured by Transwell assays. (F) Quantitative results of E. (G) Knockdown of NRG2 increased MDA-MB-231 cell migration measured by wound-healing assays (migrated section indicated in red). (H) Quantitative results of G. Data are expressed as means ± SEM from at least three experiments. $^{*}$P<0.05, $^{***}$P<0.001, $^{****}$P<0.0001. NRG2, neuroregulatory protein 2; CCK-8, Cell counting kit-8.

sh-NRG2 transfection compared with the sh-control cells (Fig. 8C and D).

## Discussion

BRCA is the predominant malignancy affecting women globally and exhibits the highest fatality rate in female patients. ATGs exert a dual influence on BRCA, as shown in previous studies where certain ATGs have been implicated in inhibiting tumorigenesis, whereas others have been found to promote tumor characteristics in malignant mammary cells (35-38). Considering the important role of autophagy in BRCA, an autophagy-related prognosis model of BRCA in TCGA dataset was constructed, and it was found that

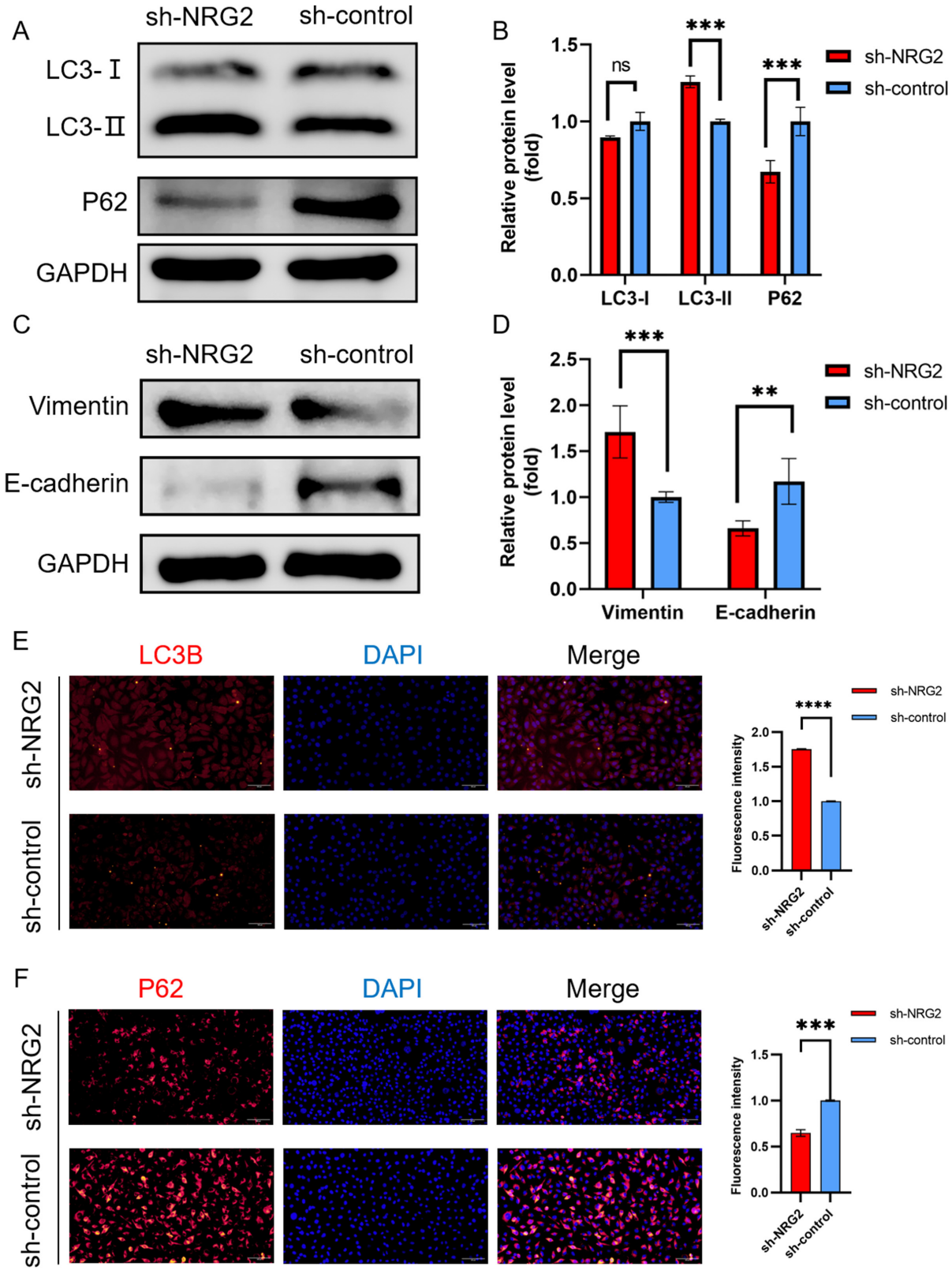


Figure 8. Knockdown of NRG2 promotes autophagy and EMT. (A) Western blot analysis of the expression levels of autophagy-related proteins LC3 and P62. (B) Quantitative results of A. (C) Western blot analysis of the expression levels of EMT-related proteins vimentin and E-cadherin. (D) Quantitative results of C. (E) LC3B (red) was prominent in cytoplasm of MDA-MB-231 cells by immunofluorescence. (F) p62 (red) was prominent in cytoplasm of MDA-MB-231 cells by immunofluorescence. Nuclei were stained with DAPI (blue). $^{**}$P<0.01, $^{***}$P<0.001, $^{****}$P<0.0001. ns; no significance; NRG2, neuroregulatory protein 2; EMT, epithelial-mesenchymal transition. LC3, light chain 3.

NRG2 served as a hub gene through the PPI network of DEATGs.

In the present study, a comprehensive bioinformatics analysis was performed to explore the potential regulatory pathways

and biological functions of NRG2 in BRCA. Additionally, the effect of NRG2 on the malignant characteristics of BRCA was verified by experiments. According to the findings, NRG2 was significantly under-expressed in patients with BRCA and may change during the early stages of BRCA. Survival analysis results revealed that the OS, PFI and DSS rate of patients with high NRG2 expression was significantly greater than that of low levels. The ROC curve indicated that low NRG2 expression has a good diagnostic value. Finally, the results of the multiple Cox regression analyses showed that low NRG2 expression is an independent risk factor for OS. The aforementioned findings indicated that NRG2 may serve as a prognostic and diagnostic biomarker for BRCA. Furthermore, the lowest expression of NRG2 was observed in the luminal B subtype comparing with luminal A, Her2 and basal subtypes, and the overall survival and ROC curve analysis revealed compelling evidence supporting the significant diagnostic and prognostic value of NRG2 specifically in the luminal B subtype.

NRG2 expression was positively correlated with most immune cells such as B cells, cytotoxic cells, $CD8^+$ T cells, dendritic cells, T cells and neutrophils, which were reduced in tumor immune microenvironments when NRG2 expression decreased. The inhibition of CD22 mediated B-cell receptor (BCR) regulation and antigen activated BCR leading to generation of second messengers in GSEA enrichment analysis may cause decrease B cell activation, B cell antigen receptor-induced proliferation and B cell turnover rates (39,40). GO-KEGG analysis also showed that the NRG2 related genes were enriched in regulation of T cell activation and chemokine activity. The TISIDB demonstrated that NRG2 might positively regulate the CX3CL1 and CXCL family especially CXCL1-6. The main function of CXCL1-6 is recruitment of immunocytes, especially neutrophils (41). The decrease of recruitment of immunocytes induced by NRG2 knockdown in BRCA also reduced immune infiltration level. Inhibiting of anti-tumoral immunity and enhancing of immune escape may be strongly correlated with oncogenic processes mediated by NRG2.

In the present study, the functional analysis in MDA-MB-231 cells demonstrated that NRG2 silencing significantly contributed to the malignant characteristics of tumor cells including cell proliferation, migration and invasion. Both the processes of autophagy and EMT are crucially involved in the invasion and metastasis of cancer cells. On one hand, autophagy provides energy vital to cancer cells and can widely modulate the EMT process. On the other hand, EMT can regulate autophagy via pathways such as WNT and NF-κB (11). The occurrence of autophagy was observed through the conversion of LC3-I to LC3-II, as well as the degradation of p62. EMT was indicative by decreased epithelial indicator E-cadherin and increased mesenchymal marker vimentin.

From the enrichment results of GO-KEGG in the present study, various pathways that are highly related to the occurrence and development of cancer were detected, such as Ras, JAK-STAT, Wnt, TNF, NF-κB and Hedgehog signaling pathway. Several investigations have demonstrated an elevated level of autophagy in cells with RAS-activating mutations which promote tumor growth, survival and oncogenesis, and are linked to the progression of certain lethal cancers (42-44). The cross-regulatory relationships between Hedgehog, Wnt and NF-κB pathways regulate the expression and function of EMT-inducing transcription factors, and in turn, affect basic cellular mechanisms such as proliferation, differentiation and survival (45-47).

GSEA enrichment results showed that transcription and DNA repair were enriched in the low-NRG2 expression group while the MAPK and NF-κB signaling pathways were enriched in high-NRG2 expression group. Copetti *et al* (48) showed that NF-κB can induce autophagy by transactivating Beclin-1, while autophagy regulation by MAPK has similarities with NF-κB. Additionally, Xu *et al* (49) proved that NF-κB and MAPK inhibitors upregulated LC3-II mRNA expression and sustained autophagy. Therefore, the autophagy mediated by knockdown of NRG2 may be caused by inhibiting the MAPK and NF-κB signaling pathway.

Although the present study has made noteworthy contributions in elucidating the role of NRG2 in BRCA, it does have the following limitations. First, the data used for analysis was from public databases. As such, although the available data was meaningful and contributes to the knowledge of the biofunction of NRG2, its function still needs further verification through *in vitro* and *in vivo* experiments. Furthermore, although the present study proved that NRG2 can promote autophagy and EMT in BRCA through bioinformatics combined with experiments, its exact mechanism and its role in other cell lines needs to be investigated in further studies.

In summary, the present study found that NRG2 is an autophagy-related prognostic biomarker, which is significantly associated with an improved prognosis. Downregulation of NRG2 may be strongly associated with oncogenic processes involving the inhibition of anti-tumor immunity and enhancement of immune evasion. The NRG2 gene may act as a tumor suppressor factor that inhibits cell proliferation, invasion and migration by regulating the pathological process of autophagy and EMT, suggesting that NRG2 could be used as a prognostic marker for clinical therapy of BRCA.

**Acknowledgements**

The authors would like to thank Dr Yuan Cao at The Medicine & Sciences Analysis Center of Wuhan University of Science and Technology (Wuhan, China) for their help with immunofluorescence imaging and analysis. The authors would also like to thank Dr Hui Li at Tianyou Hospital (Wuhan, China) for assisting in the preparation of materials for ethics approval.

**Funding**

This study was supported by the Foundation of Hubei Province Supporting Enterprise Technology Innovation Development (grant no. 2021BAB126), Wuhan East Lake High-tech Zone 'JieBangGuaShuai' Project (grant no. 2022KJB113) and Foundation of Wuhan University of Science and Technology (grant no. 2016xz036).

**Availability of data and materials**

The data generated in the present study may be requested from the corresponding author.

## Authors' contributions

RJZ and JJD executed the project, analyzed the bioinformatics data and wrote the original manuscript draft; RLZ carried out the data curation; MYW and XTD were responsible for methodology optimization, the analysis of experimental data and construction of figures; QZ, ZRW and FL performed the *in vitro* experiments using cell lines; DY assisted with the design of clinical experiment and revision of the manuscript; YX designed the whole project and critically revised the manuscript. RJZ, JJD and YX confirm the authenticity of all the raw data. All authors read and approved the final version of the manuscript.

## Ethics approval and consent to participate

Not applicable.

## Patient consent for publication

Not applicable.

## Competing interests

The authors declare that they have no competing interests.

## References


1. Torre LA, Islami F, Siegel RL, Ward EM and Jemal A: Global Cancer in Women: Burden and Trends. Cancer Epidemiol Biomarkers Prev 26: 444-457, 2017.
2. Fan L, Strasser-Weippl K, Li JJ, St Louis J, Finkelstein DM, Yu KD, Chen WQ, Shao ZM and Goss PE: Breast cancer in China. Lancet Oncol 15: e279-e289, 2014.
3. Sung H, Ferlay J, Siegel RL, Laversanne M, Soerjomataram I, Jemal A and Bray F: Global Cancer Statistics 2020: GLOBOCAN Estimates of Incidence and Mortality Worldwide for 36 Cancers in 185 Countries. CA Cancer J Clin 71: 209-249, 2021.
4. Siegel RL, Miller KD, Wagle NS and Jemal A: Cancer statistics, 2023. CA Cancer J Clin 73: 17-48, 2023.
5. Zhang L, Chen W, Liu S and Chen C: Targeting breast cancer stem cells. Int J Biol Sci 19: 552-570, 2023.
6. Yun CW and Lee SH: The roles of autophagy in cancer. Int J Mol Sci 19: 3466, 2018.
7. Levine B and Kroemer G: Biological functions of autophagy genes: A disease perspective. Cell 176: 11-42, 2019.
8. He C and Klionsky DJ: Regulation mechanisms and signaling pathways of autophagy. Annu Rev Genet 43: 67-93, 2009.
9. Jain V, Singh MP and Amaravadi RK: Amaravadi, Recent advances in targeting autophagy in cancer. Trends Pharmacol Sci 44: 290-302, 2023.
10. Debnath J, Gammoh N and Ryan KM: Autophagy and autophagy-related pathways in cancer. Nat Rev Mol Cell Biol 24: 560-575, 2023.
11. Gundamaraju R, Lu W, Paul MK, Jha NK, Gupta PK, Ojha S, Chattopadhyay I, Rao PV and Ghavami S: Autophagy and EMT in cancer and metastasis: Who controls whom? Biochim Biophys Acta Mol Basis Dis 1868: 166431, 2022.
12. Si L and Yang Z: Regulatory effects of lncRNAs and miRNAs on the crosstalk between autophagy and EMT in cancer: A new era for cancer treatment. J Cancer Res Clin Oncol 148: 547-564, 2022.
13. Babaei G, Aziz SG and Jaghi NZZ: EMT, cancer stem cells and autophagy; The three main axes of metastasis. Biomed Pharmacother 133: 110909, 2021.
14. Akalay I, Janji B, Hasmim M, Noman MZ, Thiery JP, Mami-Chouaib F and Chouaib S: EMT impairs breast carcinoma cell susceptibility to CTL-mediated lysis through autophagy induction. Autophagy 9: 1104-1106, 2013.
15. Li Z, Lu C, Wang F, Guo H, Wang Z, Yin H and Li J: Heat treatment-induced autophagy promotes breast cancer cell invasion and metastasis via TGF-β2-mediated epithelial-mesenchymal transitions. PeerJ 11: e14640, 2023.
16. Marshall C, Blackburn E, Clark M, Humphreys S and Gullick WJ: Neuregulins 1-4 are expressed in the cytoplasm or nuclei of ductal carcinoma (in situ) of the human breast. Breast Cancer Res Treat 96: 163-168, 2006.
17. Karthaus WR and Hofree M: Regenerative potential of prostate luminal cells revealed by single-cell analysis. Science 368: 497-505, 2020.
18. Trombetta D, Sparaneo A, Fabrizio FP, Di Micco CM, Rossi A and Muscarella LA: NRG1 and NRG2 fusions in non-small cell lung cancer (NSCLC): Seven years between lights and shadows. Expert Opin Ther Targets 25: 865-875, 2021.
19. Yarden Y and Sliwkowski MX: Untangling the ErbB signalling network. Nat Rev Mol Cell Biol 2: 127-137, 2001.
20. Zhao WJ, Yi SJ, Ou GY and Qiao XY: Neuregulin 2 (NRG2) is expressed in gliomas and promotes migration of human glioma cells. Folia Neuropathol 59: 189-197, 2021.
21. Li F, Shang Y, Zhang H, She J, Wang G and Sun Q: Development of a novel autophagy-related gene prognostic signature for gastric cancer. Transl Cancer Res 10: 2790-2800, 2021.
22. Hu D, Jiang L, Luo S, Zhao X, Hu H, Zhao G and Tang W: Development of an autophagy-related gene expression signature for prognosis prediction in prostate cancer patients. J Transl Med 18: 160, 2020.
23. Sepulveda JL: Using R and bioconductor in clinical genomics and transcriptomics. J Mol Diagn 22: 3-20, 2020.
24. Shannon P, Markiel A, Ozier O, Baliga NS, Wang JT, Ramage D, Amin N, Schwikowski B and Ideker T: Cytoscape: A software environment for integrated models of biomolecular interaction networks. Genome Res 13: 2498-2504, 2003.
25. Chin CH, Chen SH, Wu HH, Ho CW, Ko MT and Lin CY: cytoHubba: Identifying hub objects and sub-networks from complex interactome. BMC Syst Biol 8 (Suppl 4): S11, 2014.
26. Muggerud AA, Hallett M, Johnsen H, Kleivi K, Zhou W, Tahmasebpoor S, Amini RM, Botling J, Børresen-Dale AL, Sørlie T and Wärnberg F: Molecular diversity in ductal carcinoma in situ (DCIS) and early invasive breast cancer. Mol Oncol 4: 357-368, 2010.
27. Gruosso T, Mieulet V, Cardon M, Bourachot B, Kieffer Y, Devun F, Dubois T, Dutreix M, Vincent-Salomon A, Miller KM and Mechta-Grigoriou F: Chronic oxidative stress promotes H2AX protein degradation and enhances chemosensitivity in breast cancer patients. EMBO Mol Med 8: 527-549, 2016.
28. Vasaikar SV, Straub P, Wang J and Zhang B: LinkedOmics: Analyzing multi-omics data within and across 32 cancer types. Nucleic Acids Res 46: D956-D963, 2018.
29. Wu T, Hu E, Xu S, Chen M, Guo P, Dai Z, Feng T, Zhou L, Tang W, Zhan L, *et al*: clusterProfiler 4.0: A universal enrichment tool for interpreting omics data. Innovation (Camb) 2: 100141, 2021.
30. Walter W, Sánchez-Cabo F and Ricote M: GOplot: An R package for visually combining expression data with functional analysis. Bioinformatics 31: 2912-2914, 2015.
31. Bindea G, Mlecnik B, Tosolini M, Kirilovsky A, Waldner M, Obenauf AC, Angell H, Fredriksen T, Lafontaine L, Berger A, *et al*: Spatiotemporal dynamics of intratumoral immune cells reveal the immune landscape in human cancer. Immunity 39: 782-795, 2013.
32. Hänzelmann S, Castelo R and Guinney J: GSVA: Gene set variation analysis for microarray and RNA-seq data. BMC Bioinformatics 14: 7, 2013.
33. Ru B, Wong CN, Tong Y, Zhong JY, Zhong SSW, Wu WC, Chu KC, Wong CY, Lau CY, Chen I, *et al*: TISIDB: An integrated repository portal for tumor-immune system interactions. Bioinformatics 35: 4200-4202, 2019.
34. Livak KJ and Schmittgen TD: Analysis of relative gene expression data using real-time quantitative PCR and the 2(-Delta Delta C(T)) method. Methods 25: 402-408, 2001.
35. Niklaus NJ, Tokarchuk I, Zbinden M, Schläfli AM, Maycotte P and Tschan MP: The multifaceted functions of autophagy in breast cancer development and treatment. Cells 10: 1447, 2021.
36. Jin L, Chen Y, Cheng D, He Z, Shi X, Du B, Xi X, Gao Y and Guo Y: YAP inhibits autophagy and promotes progression of colorectal cancer via upregulating Bcl-2 expression. Cell Death Dis 12: 457, 2021.
37. Liu X, Ma B, Chen M, Zhang Y, Ma Z and Chen H: Prognostic Autophagy-Related genes of gastric cancer patients on chemotherapy. Front Genet 12: 720849, 2021.
38. Ding J, Wang C, Sun Y, Guo J, Liu S and Cheng Z: Identification of an Autophagy-Related signature for prognosis and immunotherapy response prediction in ovarian cancer. Biomolecules 13: 339, 2023.

39. Poe JC, Fujimoto Y, Hasegawa M, Haas KM, Miller AS, Sanford IG, Bock CB, Fujimoto M and Tedder TF: CD22 regulates B lymphocyte function in vivo through both ligand-dependent and ligand-independent mechanisms. Nat Immunol 5: 1078-1087, 2004.
40. Harwood NE and Batista FD: Early events in B cell activation. Annu Rev Immunol 28: 185-210, 2010.
41. Zhou C, Gao Y, Ding P, Wu T and Ji G: The role of CXCL family members in different diseases. Cell Death Discov 9: 212, 2023.
42. Gonçalves PR, Rocha-Brito KJ, Fernandes MR, Abrantes JL, Durán N and Ferreira-Halder CV: Violacein induces death of RAS-mutated metastatic melanoma by impairing autophagy process. Tumour Biol 37: 14049-14058, 2016.
43. Su H, Yang F, Fu R, Li X, French R, Mose E, Pu X, Trinh B, Kumar A, Liu J, *et al*: Cancer cells escape autophagy inhibition via NRF2-induced macropinocytosis. Cancer Cell 39: 678-693. e11, 2021.
44. Lee JJ and Jain V: Clinical translation of combined MAPK and autophagy inhibition in RAS mutant cancer. Int J Mol Sci 22: 12402, 2021.
45. Malla RR and Kiran P: Tumor microenvironment pathways: Cross regulation in breast cancer metastasis. Genes Dis 9: 310-324, 2022.
46. Gonzalez DM and Medici D: Signaling mechanisms of the epithelial-mesenchymal transition. Sci Signal 7: re8, 2014.
47. Mirzaei S, Saghari S, Bassiri F, Raesi R, Zarrabi A, Hushmandi K, Sethi G and Tergaonkar V: NF-κB as a regulator of cancer metastasis and therapy response: A focus on epithelial-mesenchymal transition. J Cell Physiol 237: 2770-2795, 2022.
48. Copetti T, Bertoli C, Dalla E, Demarchi F and Schneider C: p65/RelA modulates BECN1 transcription and autophagy. Mol Cell Biol 29: 2594-2608, 2009.
49. Xu K, Chen W, Wang X, Peng Y, Liang A, Huang D, Li C and Ye W: Autophagy attenuates the catabolic effect during inflammatory conditions in nucleus pulposus cells, as sustained by NF-κB and JNK inhibition. Int J Mol Med 36: 661-668, 2015.